

# Catalytic hydrogenation of azobenzene in the presence of a cuboidal $\text{Mo}_3\text{S}_4$ cluster *via* an uncommon sulfur-based $\text{H}_2$ activation mechanism

Eva Guillamón,<sup>§,†</sup> Mónica Oliva,<sup>§,†</sup> Juan Andrés<sup>†</sup>, Rosa Llusar,<sup>\*,†</sup> Elena Pedrajas,<sup>†</sup> Vicent S. Sa-font,<sup>†</sup> Andres G. Algarra<sup>\*,‡</sup> and Manuel G. Basallote<sup>\*,‡</sup>

<sup>†</sup> Departament de Química Física i Analítica, Universitat Jaume I, Av. Sos Baynat s/n, 12071 Castelló, Spain.

<sup>‡</sup> Departamento de Ciencia de los Materiales e Ingeniería Metalúrgica y Química Inorgánica, Facultad de Ciencias, Universidad de Cádiz, Apartado 40, Puerto Real, 11510 Cádiz, Spain.

**KEYWORDS.** cluster catalysis, density functional theory, azobenzene hydrogenation, hydrogen activation, microkinetic modelling, molybdenum sulfide, reaction mechanism

---

**ABSTRACT:** Azobenzene hydrogenation is catalyzed under moderate conditions by a cuboidal  $\text{Mo}_3(\mu_3\text{-S})(\mu\text{-S})_3$  diamino complex *via* a cluster catalysis mechanism. Dihydrogen activation by the molecular  $[\text{Mo}_3(\mu_3\text{-S})(\mu\text{-S})_3\text{Cl}_3(\text{dmen})_3]^+$  cluster cation takes place at the  $\mu\text{-S}$  bridging atoms without direct participation of the metals in clear contrast with classical concepts. The reaction occurs with formation of 1,2-diphenylhydrazine as intermediate with similar appearance and disappearance rate constants. On the basis of DFT calculations a mechanism is proposed in which formation of 1,2-diphenylhydrazine and aniline occurs through two interconnected catalytic cycles that share a common reaction step that involves  $\text{H}_2$  addition to two of the bridging sulfur atoms of the catalyst to form a dithiolate  $\text{Mo}_3(\mu_3\text{-S})(\mu\text{-SH})_2(\mu\text{-S})$  adduct. Both catalytic cycles have similar activation barriers, in agreement with the experimental observation of close rate constant values. Microkinetic modelling of the process leads to computed concentration-time profiles in excellent agreement with the experimental ones providing additional support to the calculated reaction mechanism. Slight modifications on the experimental conditions of the catalytic protocol in combination with theoretical calculations discard a direct participation of the metal on the reaction mechanism. The effect of the ancillary ligands on the catalytic activity of the cluster fully agrees with the present mechanistic proposal. The results herein demonstrate the capability of molybdenum sulfide materials to activate hydrogen through an uncommon sulfur based mechanism opening attractive possibilities towards their applications as catalysts in other hydrogenation processes.

---

Catalytic hydrogenation of organic compounds lies at the foundations of modern chemistry due to its great practical significance, and transition metal catalysts have been the most effective in achieving this transformation.<sup>1</sup> Dihydrogen activation is a key step of these catalytic processes and its mechanism has been intensively studied using both experimental and theoretical methods.<sup>2</sup> Molybdenum sulfide based materials have recently emerged as an alternative to noble metals for the hydrogenation of unsaturated substrates.<sup>3</sup> However, the mechanism of hydrogen activation at these compounds is still under debate. Indeed, a number of studies have shown that  $\text{H}_2$  adsorption characteristics of  $\text{MoS}_2$  depend on the structure (basal-plane *vs.* edge sites), its degree of sulfur saturation, hydrogen coverage and temperature.<sup>4</sup>

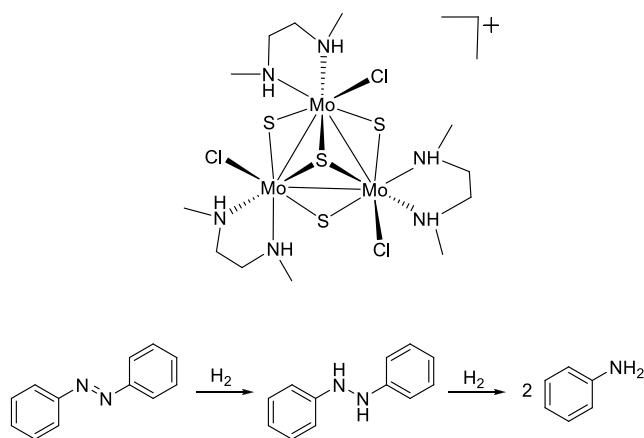
Given the difficulties associated to obtain mechanistic information on heterogeneous  $\text{MoS}_2$  based catalysts, various research groups have tackled the chemistry of homogeneous catalysis mediated by molybdenum sulfide complexes. In particular, molecular clusters represent simplified structural models of  $\text{MoS}_2$  that often emulate their catalytic properties. During the past decade we have exploited this approach by studying the behavior of trinuclear molybdenum sulfide clusters containing a cuboidal  $\text{Mo}_3(\mu_3\text{-S})(\mu\text{-S})_3$  core. Specifically, we have shown

that these species are able to catalyze the reduction of nitroarenes<sup>5</sup> and the semi-hydrogenation of alkynes.<sup>6</sup> These results prompted us to extend our studies to other unsaturated substrates, and in particular, we focused on those containing N-N bonds.

Previous studies by our group, in collaboration with Beller's group, have shown that hydrogenation of nitroarenes to afford aniline derivatives catalyzed by diamino and diimino  $\text{Mo}_3(\mu_3\text{-S})(\mu\text{-S})_3$  complexes occurs through the two competing paths proposed by Haber more than a century ago, *i.e.* the direct and the condensation routes.<sup>7</sup> The latter leads to aniline through azoxy, azo, and hydrazo derivatives, so azobenzene catalytic hydrogenation to afford aniline using  $\text{Mo}_3\text{S}_4$  clusters seems feasible. However, the mechanism of such transformation remains unclear although experimental evidences give support to the preservation of the cluster complex integrity during the catalytic transformation.

Herein, we present an efficient protocol for the azobenzene hydrogenation catalyzed by the cuboidal  $[\text{Mo}_3(\mu_3\text{-S})(\mu\text{-S})_3\text{Cl}_3(\text{dmen})_3]^+$  (**1**) complex (see Scheme 1). In our study, we combine experimental and DFT methods to unravel the kinetics of the process as well as its reaction mechanism. Our work pin-

points a homolytic H<sub>2</sub> activation mechanism at two of the bridging sulfur atoms followed by two consecutive hydrogen transfers to azobenzene and 1,2-diphenylhydrazine to afford aniline.



**Scheme 1.** Structure of the [Mo<sub>3</sub>S<sub>4</sub>Cl<sub>3</sub>(dmen)<sub>3</sub>]<sup>+</sup> (**1**) cluster cation (top) and sequential conversion of azobenzene to 1,2-diphenylhydrazine and aniline (bottom).

In this work, the hydrogenation of azobenzene is used as a probe reaction to unveil the hydrogenation mechanism mediated by cuboidal Mo<sub>3</sub>(μ<sub>3</sub>-S)(μ-S)<sub>3</sub> cluster compounds. For that purpose we selected the diamino [Mo<sub>3</sub>S<sub>4</sub>Cl<sub>3</sub>(dmen)<sub>3</sub>]Cl complex salt and used a protocol similar to that employed for the catalytic direct hydrogenation of nitroarenes.<sup>5c</sup> In a typical experiment, azobenzene (0.1 mmol) and the cluster catalyst (0.005 mmol) were dissolved in 2 mL of methanol and the vial introduced in an autoclave. Full conversion and up to 94 % yield of aniline was achieved by using a milder protocol (10 bar of H<sub>2</sub>, 60 °C for 6 h) than the one needed for the catalytic transformation of nitrobenzene to aniline (20 bar of H<sub>2</sub>, 70°C for 18 h).<sup>5c</sup> These conditions are for instance less demanding than those employed by Suzuki *et al.* using trinuclear ruthenium pentahydride clusters, while conversion and selectivity are significantly improved.<sup>8</sup> Moreover, these results demonstrate that Mo<sub>3</sub>S<sub>4</sub> clusters are capable of promoting the cleavage of the N-N bond in hydrazine derivatives, a process of relevance to nitrogen fixation.<sup>9</sup>

The kinetics of the [Mo<sub>3</sub>(μ<sub>3</sub>-S)(μ-S)<sub>3</sub>Cl<sub>3</sub>(dmen)<sub>3</sub>]Cl catalyzed hydrogenation of azobenzene in CH<sub>3</sub>OH was then monitored in a series of batch experiments. The time course of the reaction under standard conditions (60°C, 10 atm H<sub>2</sub>) is illustrated in Figure 1, which shows the typical profile for a reaction occurring *via* two consecutive kinetic steps, in which azobenzene is initially converted into 1,2-diphenylhydrazine, which then undergoes hydrogenation to afford two equivalents of aniline (Scheme 1). The absence of induction period in Figure 1 suggests that the catalyst maintains its integrity and pinpoints the [Mo<sub>3</sub>(μ<sub>3</sub>-S)(μ-S)<sub>3</sub>Cl<sub>3</sub>(dmen)<sub>3</sub>]<sup>+</sup> cluster as the active species, which was confirmed by the absence of noticeable changes in the ESI-MS spectra at the end of the reaction (Figure S2). Notably, no deuterated aniline was formed by using CD<sub>3</sub>OD as solvent, thus precluding a solvent mediated transfer hydrogenation process. Attempts to fit the kinetic profiles in Figure 1 to a model involving two consecutive kinetic steps (A → B → C)

with rate constants  $k_1$  and  $k_2$  were unsuccessful because the values of both rate constants are close to each other, and this makes undefined the preexponential terms that include the  $k_2 - k_1$  difference in the denominator.<sup>10</sup> Nevertheless, the value of  $k_1$  can be easily derived from a fit of the data for the disappearance of the starting compound (A), and yields  $k_1 = 0.42 \pm 0.03 \text{ h}^{-1}$ . The value of  $k_2$  can then be estimated by considering that at the time when the intermediate species (B) reaches its maximum concentration  $d[B]/dt = 0$  and so  $k_1 [A] = k_2 [B]$ .<sup>11</sup> Inspection of Figure 1 indicates that the intermediate reaches its maximum concentration at *ca.* 2.4 h, and at that time the percentages of A and B are both close to 35%, and therefore  $k_2 \approx k_1$ .

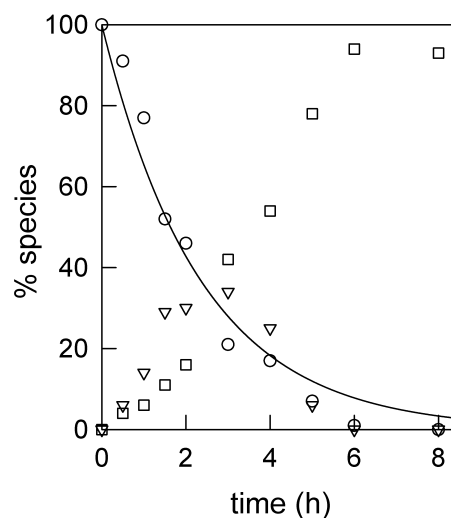


**Figure 1.** Time course for the different species observed in the catalytic hydrogenation of azobenzene: azobenzene (circles), 1,2-diphenylhydrazine (triangles) and aniline (squares). The line corresponds to the fit to a single exponential of the data for the disappearance of azobenzene.

To gain further insight into the reaction mechanism, a theoretical study on the interaction between azobenzene and the cluster was carried out. Notably, all attempts to obtain stable adducts resulting from the interaction between the cluster and azobenzene failed. Based on this outcome, the existence of cluster-hydrogen interactions was explored. However, all studied mechanisms involving H<sub>2</sub> activation with participation of the metal centers require a large energy input, unattainable under our experimental conditions (see below). This is in fact not surprising given the stability of these clusters, which feature Mo centers with an octahedral coordination environment. On the contrary, the H<sub>2</sub> molecule was found to react with two of the bridging sulfide ligands of the cluster to form a [Mo<sub>3</sub>(μ<sub>3</sub>-S)(μ-SH)<sub>2</sub>(μ-S)Cl<sub>3</sub>(dmen)<sub>3</sub>]<sup>+</sup> (**1-H<sub>2</sub>**) adduct with a reasonable energy requirement, as shown in the corresponding energy profile (Figure 2). The process is endergonic by 14.7 kcal/mol and leads to the homolytic cleavage of the H-H bond with formation of two (μ-S)-H bonds with a Gibbs energy barrier of 16.9 kcal/mol. Interestingly, this mechanism shares common features with the [3+2] cycloaddition reaction between Mo<sub>3</sub>(μ<sub>3</sub>-S)(μ-S)<sub>3</sub> clusters and alkynes to form dithiolene adducts, as in both cases a bond (either a π C-C bond of the alkyne or the σ H-H bond of dihydrogen) is broken and two new σ bonds formed (S-C and S-H, respectively).<sup>12</sup> In addition, there is a shortening of one Mo-Mo bond from 2.759 Å in **1**, typical of a single metal-metal bond,

to 2.687 Å in **1-H<sub>2</sub>**, characteristic of a double metal–metal bond (Table S1). The same tendency is observed upon alkyne insertion into the Mo<sub>3</sub>S<sub>4</sub> unit both in the experimental and in the optimized structures.<sup>12</sup> The geometry of the TS, depicted in Figure 2, shows similar (μ-S)–H bond distances as expected for a homolytic dihydrogen activation process.

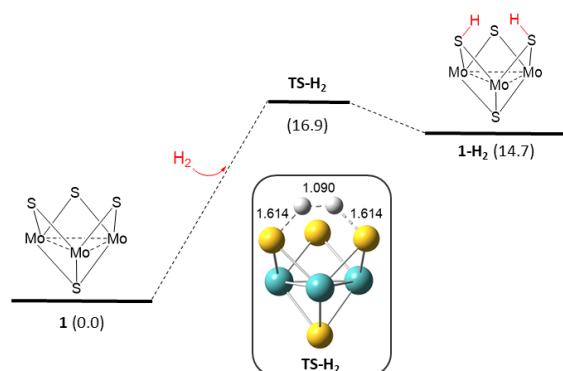


**Figure 2.** Gibbs energy profile, in kcal/mol, relative to reactants (**1**) for the addition of hydrogen to the cluster. For simplicity, dmen and Cl ligands at the Mo centres are not drawn. Blue, yellow and white spheres represent the Mo, S and H atoms, respectively.

It is worth highlighting at this point the similarities in the reactivity of [Mo<sub>3</sub>(μ<sub>3</sub>-S)(μ-S)<sub>3</sub>Cl<sub>3</sub>(dmen)<sub>3</sub>]<sup>+</sup> and the dinuclear [Cp\*Mo]<sub>2</sub>(μ-S)<sub>2</sub>(μ-S<sub>2</sub>) cluster.<sup>13</sup> The latter also reacts with H<sub>2</sub> through its bridging sulfide ligands to form the species containing two hydrosulfido ligands [Cp\*Mo]<sub>2</sub>(μ-S)<sub>2</sub>(μ-SH)<sub>2</sub>, although in this case the process is slightly exergonic.<sup>14</sup> Moreover, [Cp\*Mo]<sub>2</sub>(μ-S)<sub>2</sub>(μ-SH)<sub>2</sub> reacts at room temperature with azobenzene by transferring those two H atoms, which generates 1,2-diphenylhydrazine and regenerates the [Cp\*Mo]<sub>2</sub>(μ-S)<sub>2</sub>(μ-S<sub>2</sub>) cluster. Interestingly, at least under the milder experimental conditions employed by Dubois *et al.*, this process does not result in the formation of aniline and only one equivalent of H<sub>2</sub> is incorporated into the azobenzene molecule. In spite of such difference, the data on [Cp\*Mo]<sub>2</sub>(μ-S)<sub>2</sub>(μ-SH)<sub>2</sub> is in line with the reaction mechanism suggested by our DFT calculations for the azobenzene hydrogenation in the presence of **1**. These results indicate that the sequential formation of 1,2-diphenylhydrazine and aniline takes place through two interconnected catalytic cycles which share the formation of **1-H<sub>2</sub>** as a common step. This species, resulting from the homolytic activation of a dihydrogen molecule, is able to transfer its two hydrogen atoms to either azobenzene or 1,2-diphenylhydrazine. This can be viewed as two independent catalytic cycles in which each dihydrogen transfer regenerates the [Mo<sub>3</sub>(μ<sub>3</sub>-S)(μ-S)(μ-S)<sub>2</sub>Cl<sub>3</sub>(dmen)<sub>3</sub>]<sup>+</sup> cluster (Figure 3).

The calculated DFT profile for both cycles is shown in Figure 4. In the first cycle, the reaction between **1-H<sub>2</sub>** and azobenzene through transition state **TS-1** directly transforms the latter species into 1,2-diphenylhydrazine. Interestingly, the two H atoms transferred in **TS-1** feature distinct S–H (1.549 and 1.400 Å) and H–N (1.495 and 2.166 Å) distances, which is indicative of an asynchronous process (Figure S8). Hydrogen transfer in the

second cycle occurs in a stepwise manner through the **I-2** intermediate connected with 1,2-phenylhydrazine and aniline *via* transition states **TS-2A** and **TS-2B**, respectively. Note that the dispersion and standard state corrections required to obtain relative free energies within this cycle results in an unrealistic free energy value for **TS-2A**, as it is computed to be lower than those of **1-H<sub>2</sub>** and **I-2**. This is an artifact that appears when neighboring stationary points have similar energies and it is no present in the potential energy profile. (Figure S7). In any case, intermediate **I-2** is not relevant from a thermodynamic viewpoint nor it is expected to be experimentally observed.

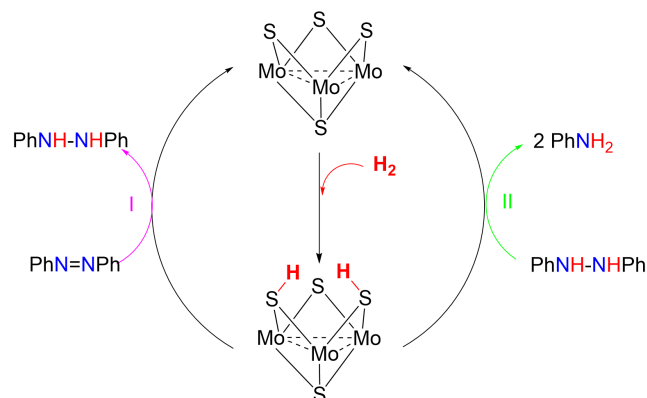


**Figure 3.** Mechanism proposed for the catalytic conversion of azobenzene into aniline. The figure illustrates the operation of two interconnected catalytic cycles, one for the hydrogenation of diazobenzene (cycle I) and another for the hydrogenation of 1,2 diphenylhydrazine (cycle II).

The data in Figure 4 indicates that overcoming transition states **TS-1** and **TS-2B** represent the rate-determining steps of each cycle. This results in Gibbs energy barriers of 18.2 and 17.7 kcal/mol, respectively, when those of the cluster, H<sub>2</sub> and nitrogen-containing substrate are taken as relative zero. This is indeed in very good agreement with the experimental observation of close rate constants for the formation of 1,2-diphenylhydrazine and its conversion to aniline. It is worth highlighting that each of these barriers results from the combination of two different processes: (a) the formation of intermediate **1-H<sub>2</sub>**, which in both cases requires 16.9 kcal/mol to overcome **TS-H<sub>2</sub>** and reach **1-H<sub>2</sub>**, which lies 14.7 kcal/mol above the starting point of each cycle; (b) the subsequent transfer of the H atoms to the substrates, which requires 3.5 and 3.0 kcal/mol in cycles I and II, respectively, to climb from **1-H<sub>2</sub>** to each limiting TS. Based on this Gibbs energy profile, the formation of **1-H<sub>2</sub>** is relatively difficult, hence the required high H<sub>2</sub> pressure and temperature. Nevertheless, once it is formed, it will react with azobenzene or 1,2-diphenylhydrazine with quite similar energy barriers. This suggests that **1-H<sub>2</sub>** will have an almost negligible discrimination capability, with the experimental observation of sequential formation of 1,2-diphenylhydrazine and aniline being just a consequence of the relative concentrations throughout the experiment. Specifically, the absence of 1,2-diphenylhydrazine at the early stages of reaction will favor the reaction with azobenzene (cycle I), but as the reaction goes on and the ratio between the concentrations of 1,2-diphenylhydrazine and azobenzene increases, cycle II will be favoured against cycle I.

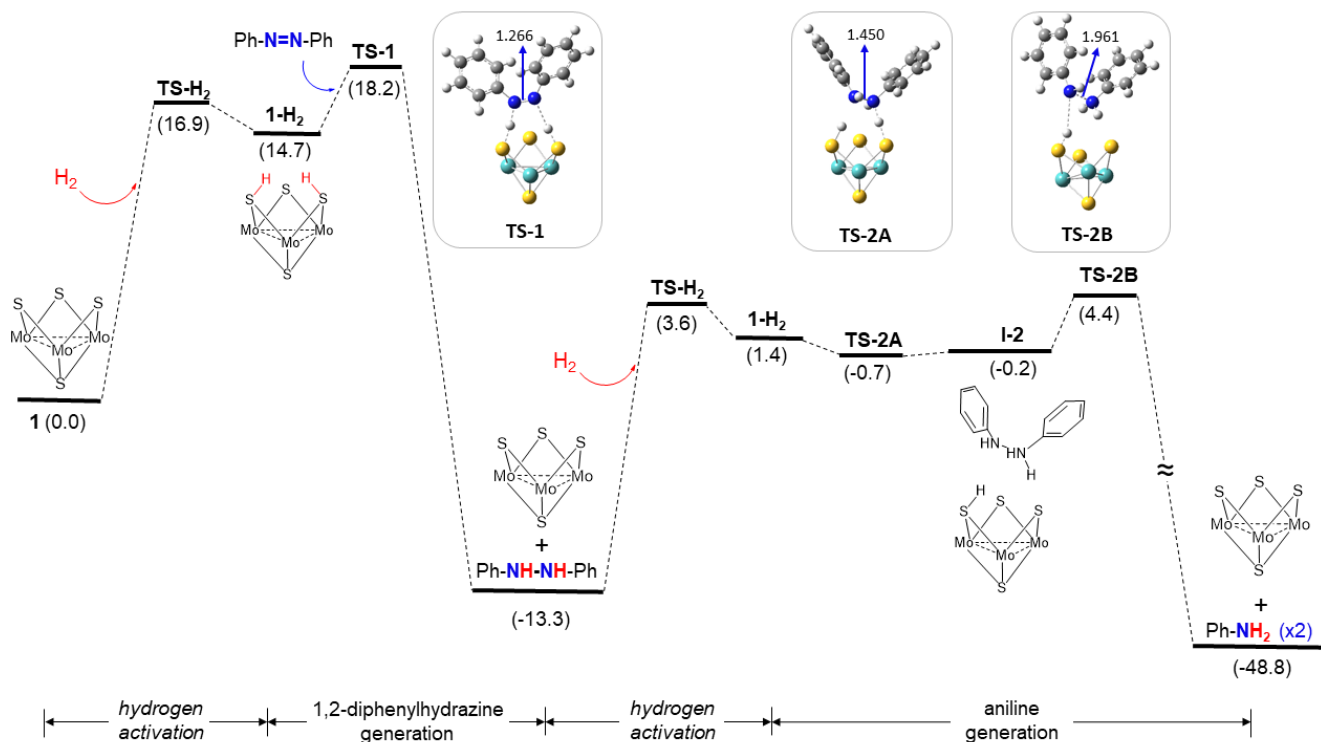


**Figure 4.** Gibbs energy profile (kcal/mol) for the two-cycle catalytic conversion of azobenzene to aniline. Cl and dmen ligands are omitted for simplicity. N–N distances at the TSs are given in Å.

The complexity of the proposed mechanism is, evidently, associated with the presence of at least five different species in the reaction mixture (cluster,  $H_2$ , azobenzene, 1,2-diphenylhydrazine and aniline). In order to evaluate how the Gibbs energy profile in Figure 4 is affected by the varying concentrations of these species, the system has been studied *via* microkinetic modeling.<sup>15</sup> For that purpose, the rate constants for the different steps were estimated from their Gibbs energies of activation in Figure 4 using the Eyring equation, which allowed the concentration-time profiles for each species to be computed. The experimental kinetic data in Figure 1 were found to be well reproduced (Figure 5) by simply introducing minor changes in the rate constant for the initial  $H_2$  addition to the cluster. Actually, a rate constant of  $1.31 \pm 0.06 \text{ M}^{-1} \text{ s}^{-1}$  was obtained by fitting the experimental data to the computed mechanism, which corresponds to a Gibbs energy of activation of  $19.4 \text{ kcal mol}^{-1}$ . This value differs from that in Figure 4 ( $16.9 \text{ kcal mol}^{-1}$ ) only by  $2.5 \text{ kcal mol}^{-1}$ , which is surely within the experimental and computational errors.

The key feature of the proposed mechanism is the activation of  $H_2$  at the bridging sulfur atoms of the cluster to form intermediate  $1\text{-H}_2$ . Unfortunately, the energy profiles show that this species is expected to be formed under steady-state conditions, and actually its concentration under the experimental conditions used is estimated to be lower than  $10^{-14} \text{ M}$  both in the presence and in the absence of azobenzene (Figure S10), which makes it undetectable. In agreement with these expectations, the NMR spectra of the cluster under  $H_2$  pressure (Figure S5), failed to observe the formation of significant amounts of any other species.

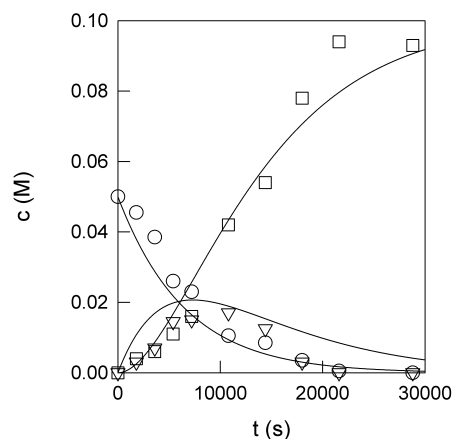


**Figure 5.** Concentration-time profiles for azobenzene (circles), 1,2-diphenylhydrazine (triangles) and aniline (squares) during the cluster-catalyzed hydrogenation process. The symbols correspond to the experimental data (Figure 1 with the percentages converted to concentrations and times in seconds), and the lines to the concentrations calculated from the computed mechanism in Figure 4 using the refined value of the rate constant for  $H_2$  addition to the cluster ( $1.31 \text{ M}^{-1} \text{ s}^{-1}$ ).

Given the impossibility of detecting the  $1\text{-H}_2$  intermediate, we directed our efforts to find indirect experimental evidences which could provide support to the above sulfur centered mechanism and simultaneously discard any metal participation in the process. A clear evidence supporting  $H_2$  activation by the bridging

ing sulfur atoms in **1** was obtained by blocking the three bridging sulfur atoms of the cluster. For that purpose, CuCl was added to the reaction mixture during the catalytic protocol (Table 1, entry 2), which resulted in the inhibition of the hydrogenation process. It is well known that cuboidal  $\text{Mo}_3(\mu_3\text{-S})(\mu\text{-S})_3$  clusters interact with a variety of metals ( $\text{M}'$ ) to form  $\text{Mo}_3\text{M}'\text{S}_4$  clusters with cubane type structures.<sup>16</sup> In this case, copper addition results in the *in situ* formation of the heterobimetallic  $[\text{Mo}_3(\text{CuCl})\text{S}_4\text{Cl}_3(\text{dmen})_3]^+$  cation, which was isolated as the  $\text{CuCl}_2^-$  salt whose crystal structure (Figure S6) shows the formation of three new  $(\mu_3\text{-S})\text{-Cu}$  bonds.

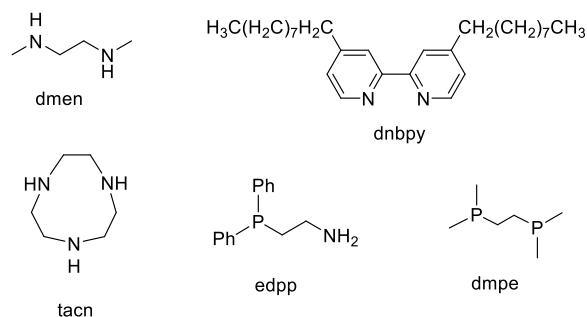
Next, a combined experimental and theoretical approach was undertaken aimed to analyze any potential mechanisms which involve the formation of vacant sites at the metal center such as dissociation of the outer halide, partial decoordination of the diamino bidentate ligand or HCl elimination with the concomitant formation of  $\text{Mo}=\text{NCH}_3$  bonds induced by a base. Performance of the catalytic protocol in the presence of added chloride (Table 1, entries 3 and 4) has no significant effect in the reaction outcome, discarding a mechanism involving a reversible dissociation-coordination of the chloride ancillary ligands that would allow for the heterolytic activation of  $\text{H}_2$  at a  $\text{Mo}-\mu\text{-S}$  bond to form a  $\text{MoH}/\text{SH}$  intermediate. In addition, no loss of the cluster  $\text{C}_3$  symmetry is observed by proton NMR when the cluster catalyst is heated under hydrogen pressure (Figure S5) as expected for a cluster containing partially de-coordinated ligands. These experimental results are further supported by theoretical calculations (Figure S11a). The alternative possibility of creating a vacant coordination site at the metal through dissociation of one of the nitrogen atoms of the diamine can also be discarded on the basis of the aforementioned cluster  $\text{C}_3$  symmetry preservation and it is also corroborated by theoretical calculations. (Figure S11b). On the other hand, HCl elimination to furnish  $\text{Mo}=\text{NCH}_3$  species that could yield  $\text{MoH}/\text{NH}$  species upon hydrogenation can also be ruled out, as calculations indicate that HCl elimination to form  $\text{Mo}=\text{NCH}_3$  species present a barrier of 39.5 kcal/mol, again much higher than that evaluated for the proposed mechanism (Figure S11c). In addition, the effect of added basis (Table 1, entries 5-7) do not support any mechanism involving HCl elimination.

With regard to the effect of added basis, pyridine addition has no significant effect in conversion and product distribution (Table 1, entry 5, see also Figure S3). However, a striking effect is found upon addition of the stronger  $\text{NEt}_3$  base, which completely inhibits the catalytic process (Table 1, entries 6-7) Under these conditions, partial substitution of one or two of the outer chlorides by methoxy and hydroxo groups is observed by ESI-MS mass spectrometry (Figure S4). The calculated  $\Delta G$  of 15.7 kcal  $\text{mol}^{-1}$  for the hydrogenation of the most abundant substitution product,  $[\text{Mo}_3\text{S}_4\text{Cl}(\text{OH})_2(\text{dmen})_3]^+$ , only shows a modest increase with respect to that of **1** to form **1-H<sub>2</sub>**. Even though these substitution compounds could have a lower catalytic activity, this would not explain the complete inhibition of the catalytic process because most of the starting cluster remains unreacted under these conditions. Indeed, a plausible explanation can be given on the basis of the proposed mechanism, as the S-H groups of the **1-H<sub>2</sub>** intermediate are expected to have acidic character (calculated pKa of 4.1), and therefore the base would capture these H atoms thereby introducing an efficient additional reaction pathway for this intermediate that would lead to inhibition of the whole hydrogenation process.

**Table 1.** Evaluation of conditions for azobenzene (AZ) hydrogenation.<sup>a</sup>

entry	variation from "initial conditions"	conversion (%) <sup>b</sup>	yield (%) <sup>b</sup>		$\Delta G^c$
			DPH	AN	
1	None	83	25	54	14.7
2	addition of CuCl (2 equiv)	0	0	0	
3	addition of (n-Bu <sub>4</sub> N)Cl (3 equiv)	82	24	55	
4	addition of (n-Bu <sub>4</sub> N)Cl (30 equiv)	80	19	45	
5	addition of pyridine (2-12 equiv)	78	19	51	
6	addition of Et <sub>3</sub> N (1 equiv)	10	4	6	
7	addition of Et <sub>3</sub> N (2-3 equiv)	0	0	0	
8	$[\text{Mo}_3\text{S}_4\text{Br}_3(\text{dmen})_3]^{+d}$	78	34	36	14.1
9	$[\text{Mo}_3\text{S}_4\text{Cl}_3(\text{dnbpy})_3]^{+d}$	14	3	11	16.2
10	$[\text{Mo}_3\text{S}_4(\text{tacn})_3]^{4+d} + \text{HBF}_4$ (1.5 equiv)	32	12	20	13.8
11	$[\text{Mo}_3\text{S}_4\text{Cl}_3(\text{edpp})_3]^{+d}$	0	0	0	21.7
12	$[\text{Mo}_3\text{S}_4\text{Cl}_3(\text{dmpe})_3]^{+d}$	0	0	0	18.3
13	$[\text{Mo}_3\text{S}_4\text{H}_3(\text{dmpe})_3]^{+d}$	0	0	0	23.5

<sup>a</sup> Reaction conditions: AZ (0.1 mmol),  $\text{CH}_3\text{OH}$  (2 mL). <sup>b</sup> Determined by GC analysis using *n*-hexadecane as an internal standard. <sup>c</sup> Computed free energy of the corresponding  $\text{Mo}_3\text{S}_4\text{-H}_2$  adduct (kcal  $\text{mol}^{-1}$ ) quoted relative to the  $\text{Mo}_3\text{S}_4$  catalyst +  $\text{H}_2$  (entries 1 and 8-13). <sup>d</sup> Outer ligands:



At that point, we decided to explore the effect of the ancillary ligands on the catalytic activity of a series of  $\text{Mo}_3\text{S}_4$  clusters decorated with diamino, diimino, triamino, aminophosphino and diphosphino ligands, aimed to gather additional arguments to this uncommon hydrogen activation mechanism at the sulfur centers. A summary of the results is listed in Table 1 (entries 8-13) together with the calculated free energy needed for the formation of the corresponding  $\text{Mo}_3\text{S}_4\text{-H}_2$  intermediates, the first and key step in the azobenzene hydrogenation reaction. To our

delight, we found a good correlation between the evaluated catalytic activity and the free energy needed to reach the  $\text{Mo}_3\text{S}_4\text{-H}_2$  intermediate in all complexes containing bidentate ligands, which provides strong support to the proposed mechanism. In particular, all clusters containing phosphorous atoms bound to the metal (Table 1, entries 11-13) are inactive. Diamino clusters show higher activities than their diimino counterparts (Table 1, entries 8-10) and substitution of chlorine by bromine in  $[\text{Mo}_3\text{S}_4\text{Cl}_3(\text{dmen})_3]^+$  (Table 1, entries 1 and 8) decreases by *ca.* 10 % the azobenzene conversion. The catalytic protocol for the triazacyclononane  $\text{Mo}_3\text{S}_4$  derivative (Table 1, entry 10) was performed in the presence of acid to avoid deprotonation of the coordinated tacn ligands, as it has been shown that cluster salts of the  $[\text{Mo}_3\text{S}_4(\text{tacn})_3]^{4+}$  cation can only be crystallized from acidic solutions ( $\text{pH} < 2$ ).<sup>17</sup> Under these conditions, conversions lye between those obtained for the diamino and the diimino cluster catalysts.

A definite proof in favor of our sulfur centered mechanistic proposal comes from the observed catalytic activity when capping the molybdenum atoms with tacn ligands. In the structure of  $[\text{Mo}_3\text{S}_4(\text{tacn})_3]^{4+}$ , the three outer positions on each metal are completed by facially coordinating tridentate macrocyclic tacn amine ligands. This circumstance indicates that formation of a Mo-based reaction site is highly unlikely. In contrast, as detailed before, blocking of the sulfur atoms (Table 1, entry 2) results in the inhibition of the catalytic hydrogenation of azobenzene.

In conclusion, the  $[\text{Mo}_3\text{S}_4\text{Cl}_3(\text{dmen})_3]^+$  cuboidal cluster efficiently catalyzes the reduction of azobenzene to aniline with high yields under relatively mild conditions. The reaction occurs with formation of 1,2-diphenylhydrazine as a detectable intermediate, which is formed and disappears with close rate constants. Experimental outcomes, computational studies and microkinetic modelling support a reaction mechanism in which  $\text{H}_2$  is homolytically activated at two of the three bridging sulfur atoms of the cluster to form a dithiol  $[\text{Mo}_3(\mu_3\text{-S})(\mu\text{-S})(\mu\text{-SH})_2\text{Cl}_3(\text{dmen})_3]^+$  intermediate under steady-state conditions. This intermediate is able to transfer both hydrogen atoms to azobenzene and to 1,2-diphenylhydrazine through two interconnected catalytic cycles. Although all processes take place without direct participation of the Mo centers or their ancillary ligands, the latter are found to significantly modulate the ability of the cluster to activate the  $\text{H}_2$  molecule and ultimately catalyze the hydrogenation of azobenzene. The proposed mechanism represents a new example of activation of small molecules at the bridging sulfur atoms triangle present in cuboidal  $\text{Mo}_3\text{S}_4$  clusters. Interestingly, whereas the previously reported semihydrogenation of alkynes involves the activation of the substrate at the bridging sulfide ligands,<sup>6</sup> in the present case those ligands are employed to initially cleave the  $\sigma$  H-H bond of  $\text{H}_2$ . All in all, the results herein highlight the capability of these clusters to catalyze the hydrogenation of substrates with initial activation of either  $\text{H}_2$  or the substrate. In light of these new findings, we are currently investigating the hydrogenation of other unsaturated substrates and the results obtained will be reported in due form. Finally, it is worth noting that based on the structural similarity between  $\text{Mo}_3\text{S}_4$  clusters and the basal plane of  $\text{MoS}_2$ , which also display sulfur atoms triangles linked through Mo atoms, the catalytic potential of  $\text{MoS}_2$ -based materials in hydrogenation processes deserves further studies.

## ASSOCIATED CONTENT

**Supporting Information.** Detailed synthetic and experimental procedures, cluster monitoring, crystal structure determination, computational details, experimental and optimized bond distances of 1 and 1- $\text{H}_2$ , potential energy profile, optimized structures of TS1, TS-2A, I-2 and TS-2B, microkinetic modeling, computational tests on alternative paths and cartesian coordinates of all optimized structures. This material is available free of charge *via* the Internet at <http://pubs.acs.org>.

## AUTHOR INFORMATION

### Corresponding Authors

**Rosa llusar** - Departament de Química Física i Analítica, Universitat Jaume I, Av. Sos Baynat s/n, 12071 Castelló, Spain  
orcid.org/0000-0002-3539-7269

E-mail: [rosa.llusar@uji.es](mailto:rosa.llusar@uji.es)

**Andrés G. Algarrá** - Departamento de Ciencia de los Materiales e Ingeniería Metalúrgica y Química Inorgánica, Facultad de Ciencias, Universidad de Cádiz, Apartado 40, Puerto Real, 11510 Cádiz, Spain  
orcid.org/0000-0002-5062-2858

E-mail: [andres.algarra@uca.es](mailto:andres.algarra@uca.es)

**Manuel G. Basallote** - Departamento de Ciencia de los Materiales e Ingeniería Metalúrgica y Química Inorgánica, Facultad de Ciencias, Universidad de Cádiz, Apartado 40, Puerto Real, 11510 Cádiz, Spain  
orcid.org/0000-0002-1802-8699

E-mail: [manuel.basallote@uca.es](mailto:manuel.basallote@uca.es)

### Authors

**Eva Guillaón** - Departament de Química Física i Analítica, Universitat Jaume I, Av. Sos Baynat s/n, 12071 Castelló, Spain

**Mónica Oliva** - Departament de Química Física i Analítica, Universitat Jaume I, Av. Sos Baynat s/n, 12071 Castelló, Spain

**Juan Andrés** - Departament de Química Física i Analítica, Universitat Jaume I, Av. Sos Baynat s/n, 12071 Castelló, Spain

**Elena Pedrajas** - Departament de Química Física i Analítica, Universitat Jaume I, Av. Sos Baynat s/n, 12071 Castelló, Spain

**Vicent S. Safont** - Departament de Química Física i Analítica, Universitat Jaume I, Av. Sos Baynat s/n, 12071 Castelló, Spain

### Author Contributions

<sup>§</sup> These authors contributed equally to this work.

### Notes

The authors declare no competing financial interest.

## ACKNOWLEDGMENT

Financial support from the Spanish Ministerio de Ciencia, Innovación y Universidades for projects PGC2018-094417-B-I00 (E. G., M. O., J. A., R. L. and V. S. S.) and PID2019-107006GB-C22 (A. G. A. and M. G. B.) is gratefully acknowledged. E. G., M. O., J. A., R. L., E. P. and V. S. S. acknowledge Universitat Jaume I for projects UJI-2017-44 and UJI-B2019-30. A. G. A. and M. G. B. acknowledge the 2014-2020 ERDF Operational Programme and the Department of Economy, Knowledge, Business and University of the Regional Government of Andalusia for the project FEDER-UCA18-106840. The authors also thank the Universidad de Cádiz and the Universitat Jaume I for computational resources and the SCIC of the Universitat Jaume I for providing us with NMR, mass spectrometry and X-ray diffraction techniques. We acknowledge the ICIQ NMR Unit staff and Dr. M. Giménez for their assistance with the high pressure NMR experiments.

## ABBREVIATIONS

dmen, N,N'-dimethylethylenediamine; Cp\*, pentamethylcyclopentadienyl.

## REFERENCES

- (1) Rylander, P. N. *Catalytic Hydrogenation in Organic Syntheses*, Academic Press, New York, 1979.
- (2) Kubas, G. J.; Heinekey, D. M. Activation of Molecular Hydrogen. In *Physical Inorganic Chemistry*; John Wiley & Sons, 2010; pp 189-245.
- (3) (a) Mao, J.; Wang, Y.; Zheng, Z.; Deng, D. The rise of two-dimensional MoS<sub>2</sub> for catalysis. *Front. Phys.* **2018**, *13*, 138118; (b) Drescher, T.; Niefind, F.; Bensch, W.; Grünert, W. Sulfide Catalysis without Coordinatively Unsaturated Sites: Hydrogenation, Cis–Trans Isomerization, and H<sub>2</sub>/D<sub>2</sub> Scrambling over MoS<sub>2</sub> and WS<sub>2</sub>. *J. Am. Chem. Soc.* **2012**, *134*, 18896-18899; (c) Li, Z.; Zhang, D.; Ma, J.; Wang, D.; Xie, C. Fabrication of MoS<sub>2</sub> microflowers for hydrogenation of nitrobenzene. *Mat. Lett.* **2018**, *213*, 350-353.
- (4) (a) Kronberg, R.; Hakala, M.; Holmberg, N.; Laasonen, K. Hydrogen adsorption on MoS<sub>2</sub>-surfaces: a DFT study on preferential sites and the effect of sulfur and hydrogen coverage. *Phys. Chem. Chem. Phys.*, **2017**, *19*, 16231-16241; (b) Prodhomme, P.-Y.; Raybaud, P.; Toulhoat, H. Free-energy profiles along reduction pathways of MoS<sub>2</sub> M-edge and S-edge by dihydrogen: A first principles study. *J. Catal.* **2011**, *280*, 178–195; (c) Sun, M.; Nelson, A. E.; Adjaye, J. Adsorption and dissociation of H<sub>2</sub> and H<sub>2</sub>S on MoS<sub>2</sub> and NiMoS catalysts, *Cat. Today* **2005**, *105*, 36-43; (d) Travert, A.; Nakamura, H.; van Santen, R. A.; Cristol, S.; Paul, J.-F.; Payen E. Hydrogen Activation on Mo-Based Sulfide Catalysts, a Periodic DFT Study, *J. Am. Chem. Soc.* **2002**, *124*, 7084-7095.
- (5) (a) Sorribes, I.; Wienhöfer, G.; Vicent, C.; Junge, K.; Llusar, R.; Beller, M. Chemoselective Transfer Hydrogenation to Nitroarenes Mediated by Cubane-Type Mo<sub>3</sub>S<sub>4</sub> Cluster Catalysts. *Angew. Chem. Int. Ed.* **2012**, *51*, 7794-7798; (b) Pedrajas, E.; Sorribes, I.; Junge, K.; Beller, M.; Llusar, R. A Mild and Chemoselective Reduction of Nitro and Azo Compounds Catalyzed by a Well-Defined Mo<sub>3</sub>S<sub>4</sub> Cluster Bearing Diamine Ligands. *ChemCatChem* **2015**, *7*, 2675-2681; (c) Pedrajas, E.; Sorribes, I.; Gushchin, A. L.; Laricheva, Y. A.; Junge, K.; Beller, M.; Llusar, R. Chemoselective Hydrogenation of Nitroarenes Catalyzed by Molybdenum Sulfide Clusters. *ChemCatChem* **2017**, *9*, 1128-1134; (d) Pedrajas, E.; Sorribes, I.; Guillamón, E.; Junge, K.; Beller, M.; Llusar, R. Efficient and Selective N-Methylation of Nitroarenes under Mild Reaction Conditions. *Chem. Eur. J.* **2017**, *23*, 13205-13212; (e) Pedrajas, E.; Sorribes, I.; Junge, K.; Beller, M.; Llusar, R. Selective reductive amination of aldehydes from nitro compounds catalyzed by molybdenum sulfide clusters. *Green Chem.* **2017**, *19*, 3764-3768.
- (6) Algarra, A. G.; Guillamón, E.; Andrés, J.; Fernández-Trujillo, M. J.; Pedrajas, E.; Pino-Chamorro, J. Á.; Llusar, R.; Basallote, M. G. Cuboidal Mo<sub>3</sub>S<sub>4</sub> Clusters as a Platform for Exploring Catalysis: A Three-Center Sulfur Mechanism for Alkyne Semihydrogenation. *ACS Catal.* **2018**, *8*, 7346-7350.
- (7) Haber, F. Über stufenweise Reduktion des Nitrobenzols mit begrenztem Kathodenpotential. *Z. Elektrochem.* **1898**, *4*, 506-514.
- (8) Nakajima Y.; Suzuki, H. Nitrogen–Nitrogen Double Bond Cleavage of Azobenzene by a Triruthenium Pentahydrido Complex, (Cp'Ru)<sub>3</sub>(μ<sub>3</sub>-H)<sub>2</sub>(μ-H)<sub>3</sub>(Cp' = η<sup>5</sup>-C<sub>5</sub>Me<sub>5</sub>), and Catalytic Hydrogenation of Azobenzene and 1,2-Diphenylhydrazine. *Organometallics* **2005**, *24*, 1860-1866.
- (9) (a) Tanifuji, K.; Ohki, Y. Metal–Sulfur Compounds in N<sub>2</sub> Reduction and Nitrogenase-Related Chemistry, *Chem. Rev.* **2020**, *120*, 5194-5251; (b) Ohki, Y.; Uchida, K.; Tada, M.; Cramer, R. E.; Ogura, T.; Ohta, T. N<sub>2</sub> activation on a molybdenum–titanium–sulfur cluster, *Nat. Commun.*, **2018**, *9*, 3200.
- (10) Wilkins, R. G. Kinetics and Mechanism of Reactions of Transition Metal Complexes, 2nd Edition; Wiley-VCH, 1991.
- (11) Hendry, P.; Sargeson, A. M. Intramolecular phosphoryl transfer: chelated phosphoramidate. *Inorg. Chem.* **1986**, *25*, 865-869.
- (12) (a) Algarra, A. G.; Basallote, M. G. Computational Insights Into the Reactivity at the Sulfur Atoms of M<sub>3</sub>S<sub>4</sub> (M = Mo, W) Clusters: The Mechanism of [3 + 2] Cycloaddition With Alkynes. In *Adv. Inorg. Chem.*, Elsevier: 2017; Vol. 70, pp 311-342; (b) Pino-Chamorro, J. Á.; Gushchin, A. L.; Fernández-Trujillo, M. J.; Hernández-Molina, R.; Vicent, C.; Algarra, A. G.; Basallote, M. G. Mechanism of [3+2] Cycloaddition of Alkynes to the [Mo<sub>3</sub>S<sub>4</sub>(acac)<sub>3</sub>(py)<sub>3</sub>][PF<sub>6</sub>] Cluster. *Chem. Eur. J.* **2015**, *21*, 2835-2844.
- (13) Casewit, C. J.; Coons, D. E.; Wright, L. L.; Miller, W. K.; Dubois, M. R. Homogeneous Reductions of Nitrogen-Containing Substrates Catalyzed by Molybdenum (IV) Complexes with μ-Sulfido Ligands. *Organometallics* **1986**, *5*, 951-955.
- (14) Algarra, A. G. Computational Insights into the Mechanisms of H<sub>2</sub> Activation and H<sub>2</sub>/D<sub>2</sub> Isotope Exchange by Dimolybdenum Tetrasulfide Complexes. *Eur. J. Inorg. Chem.* **2016**, 1886-1894.
- (15) Besora M.; Maseras, F. Microkinetic modeling in homogeneous catalysis. *Wiley Interdiscip. Rev.: Comput. Mol. Sci.* **2018**, *8*, No. e1372.
- (16) Hernandez-Molina, R.; Sokolov, M. N.; Sykes, A. G. Behavioral Patterns of Heterometallic Cuboidal Derivatives of [M<sub>3</sub>Q<sub>4</sub>(H<sub>2</sub>O)<sub>9</sub>]<sup>4+</sup> (M = Mo, W; Q = S, Se). *Acc. Chem. Res.* **2001**, *34*, 223-230.
- (17) Cotton, F. A.; Dori, Z.; Llusar, R.; Schwotzer, W. Oxidative fragmentation of the cuboid molybdenum-sulfur Mo<sub>4</sub>S<sub>4</sub> cluster core: synthesis and structures of [Mo<sub>3</sub>(μ<sub>3</sub>-S)(μ-S)<sub>3</sub>([9]aneN<sub>3</sub>)<sub>3</sub>]<sup>4+</sup> and {[MoO([9]aneN<sub>3</sub>)<sub>2</sub>(μ-S)<sub>2</sub>]<sup>2+</sup> ([9]aneN<sub>3</sub> = 1,4,7-triazacyclononane)}. *Inorg. Chem.* **1986**, *25*, 3654-3658.

For TOC

